Journal of Superconductivity and Novel Magnetism (2018) 31:2019–2025
https://doi.org/10.1007/s10948-017-4470-1

ORIGINAL PAPER

Abnormal Transport and Magnetic Properties Induced by Change of the Phase Volume Ratio for $YBa_2Cu_3O_{7-\delta}/La_{0.67}Sr_{0.33}MnO_3$ Hybrids

Changzhao Chen[1] · Wuqiong Zhang[1] · Shiwang Zhu[1] · Chuanbing Cai[2]

Received: 2 August 2017 / Accepted: 28 November 2017 / Published online: 5 December 2017

Abstract

Two elaborately designed hybrids consisting of superconducting $YBa_2Cu_3O_{7-\delta}$ (YBCO) and ferromagnetic $La_{0.67}Sr_{0.33}MnO_3$ (LSMO), namely $20 \times (YBCO(m)/LSMO(100 - m))$ are prepared on single crystal $SrTiO_3$ (STO) by pulsed laser deposition (PLD) with 20 being repetition periods and $m = 90$ and 10, respectively, which represents YBCO pulse number in a period. The films show highly *c*-oriented and epitaxial quality, suggested by XRD θ–2θ scans and pole figures. The $20 \times$ (YBCO90/LSMO10) sample with a large YBCO volume fraction exhibits the typical character of a metal superconductor at about 90 K, while its transition width reaches 9.1 K, which is nearly eight times of that of the pure YBCO film. Above the superconducting transition temperature, a superparamagnetic signal rather than ferromagnetic behavior is observed, which may be associated with a diluted system consisting of the ferromagnetic nanoparticles embedded in the superconducting films. For the hybrid with a small YBCO volume fraction, i.e., the $20 \times$ (YBCO10/LSMO90) sample, its transport behavior at normal state is insulating, and it is found that the Mott variable range hopping conduction dominates in this insulating phase in the temperature range 70–310 K. Obviously distinguishable insulator to superconductor (IS) transition occurs at 52 K, but the superconducting diamagnetic signals are very weak in the magnetic measurements below the IS temperature. For this sample, the magnetization loop at 100 K is ferromagnetic, yet manifested by a reduced coercive field and residual magnetization as compared with a pure LSMO film. In fact, both hybrids represent two kinds of nanocomposites, i.e., superconducting nanoparticles in a ferromagnetic matrix and ferromagnetic nanoparticles in a superconducting matrix, which benefits to study interfacial interactions due to an increased interface to value ratio and reduced size effect.

Keywords YBCO/LSMO · Abnormal transport properties · Superparamagnetic

1 Introduction

The interplay between superconductivity (SC) and ferromagnetism (FM) has attracted very much interest yielding to both fundamental physics and new phenomena for potential applications [1, 2]. Heterostructures consisting of high-temperature superconducting $YBa_2Cu_3O_{7-\delta}$ (YBCO) and ferromagnetic half-metal $La_{0.67}Sr(Ca)_{0.33}MnO_3$ (LS(C)MO) serve as an idea platform to provide unique possibilities of combining the mutually exclusive FM and SC orders due to the low carrier density of YBCO, the nearly 100% polarization of LS(C)MO charge carriers as well as the structural and chemical similarities of both materials. In the past few years, YBCO/LS(C)MO multilayers and superlattices have been extensively studied to understand the complicated interactions between these two antagonistic long-range orderings [3–11]. By tuning some important parameters such as the thicknesses of the constituent layers, the strength and direction of the external magnetic field, a lot of phenomena have been observed including the interfacial charge transfer and reconstruction [5, 6, 10], long-range proximity effect [7, 12], the giant magnetoresistance effect [3], etc., manifesting the very important role played by the tunneling of Cooper pairs or injection of the spin-polarized carriers.

✉ Changzhao Chen
czch68@163.com

[1] College of Mechanics and Optoelectronic Physics, Anhui University of Science and Technology, Huainan 232001, China

[2] Shanghai Key Laboratory of High Temperature Superconductors, Shanghai University, Shanghai 200444, China

It is important to note that in these heterostructures, the thickness of the constituent layer is usually limited to several nanometers to obtain an observable coupling phenomenon since the characteristic lengths of numerous electronic processes across interfaces are less than 10 nm, even below 1 nm [13, 14]. Obviously, the size effect [15] due to the reduced unit layer thickness will take effect, which sets an obstacle in the path of understanding the competition between these orders and for their use in practical applications. In order to overcome the size effect, another research line attracting considerable attention is fabrication of SC/FM hybrids in the form of ferromagnetic nanoparticles of large size even mesocrystals embedded in a SC matrix. In addition to avoid the size effect, this system is also supposed to have a great increase of the interface to volume ratio, which can produce unique properties and phenomenal changes when one of the phases is allowed to break into nanometer sizes. Suresh et al. [16] reported a crossover between superconductivity and magnetism in $SrRuO_3$ mesocrystal-embedded YBCO matrix, which is explained as competing interactions between these two ordered phases. Bartolomé et al. [17] successfully fabricated hybrid YBCO/FM nanocomposite epitaxial thin films with performed spinel ferrite (MFe_2O_4, M = Mn, Co) as starting FM materials by a chemical solution deposition technique. Similar hybrids like YBCO/Fe_2O_3, YBCO/$CoFe_2O_4$, and YBCO/$YFeO_3$, have also been reported, but they are all bound to grow by physical methods [18–20]. In spite of the diversity in deposition method, the hybrid nanocomposites described above can be used to study some fundamental issues such as the nucleation of superconductivity and the mechanisms of magnetic vortex pinning.

In this work, two kinds of YBCO/LSMO nanocomposites, i.e., YBCO nanoparticles embedded in LSMO matrix and LSMO nanoparticles embedded in YBCO matrix, are prepared with respect to investigate the mutual influences between superconductivity and magnetism. Earlier work, which mostly deals with a hybrid of FM nanostructures in the YBCO matrix, is mainly focused on the effect of the ferromagnetism on superconductivity, while the inverse influence has little attention. The present hybrids combine the good compatibility of the two materials with the increased number of YBCO/LSMO interfaces, making it possible to disclose the coupling effects and open up a new avenue to manipulate the interactions of superconductivity and ferromagnetism.

2 Experimental

Two elaborately designed YBCO/LSMO hybrids are prepared on single crystal (100) $SrTiO_3$ (STO) by pulsed laser deposition (PLD). The hybrids, namely as 20 × (YBCO(m)/LSMO(100 − m)), where 20 is the repetition period and m represents the YBCO pulse number in a period which equals to 90 and 10, and the corresponding samples are termed as 20 × (Y90/L10) and 20 × (Y10/L90), respectively. During the deposition, the laser is fired alternatively on the stoichiometric targets of YBCO and LSMO with the repetition rate of 2 Hz and the energy density of about 2.0 J/cm^2. The details for sample preparation can be found elsewhere [21]. The film thickness controlled by the pulse number is measured by Alpha-step IQ profilers through mask method, indicating that the deposition rates for LSMO and YBCO are about 0.4 and 1 Å/pulse, respectively. During the film deposition, several pulses of YBCO or LSMO give island-like nanoparticles rather than a complete layer. This is because 10 pulses of YBCO give roughly 1 nm, which is less than the thickness of one YBCO unit cell (about 1.2 nm). For LSMO, 10 pulses gives the thickness close to a LSMO unit cell of 0.4 nm, but it is still difficult to form a complete layer due to the fluctuation effect in film growth. In addition, a pure YBCO and LSMO films as reference samples are prepared with the same conditions. The thicknesses of the pure YBCO and LSMO films are estimated to be 200 and 80 nm, respectively, since both have the same total pulse number of 2000 as the hybrids. Correspondingly, the two pure films are named as Y200, and L80, respectively.

Structural measurements are carried out on a four-circle x-ray diffractometer (XRD) with Cu Kα radiation. Transport and magnetic transport measurements are performed in a cryostat equipped with a 9 T magnet (Quantum Design PPMS-9T). The magnetic hysteresis loops at different temperatures are measured with applied magnetic field parallel to the c-axis of the sample.

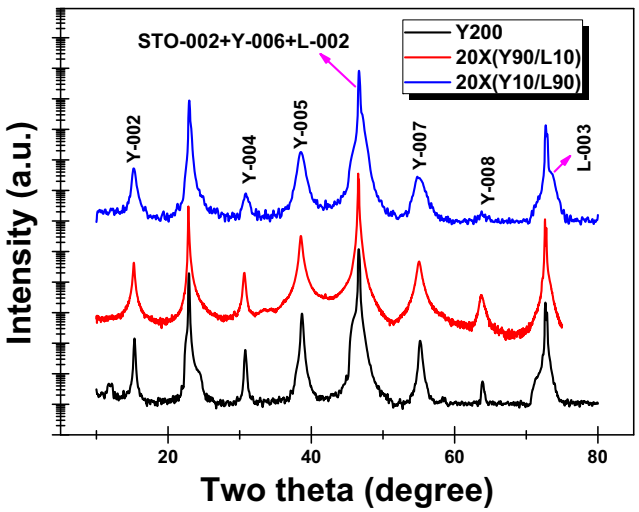

Fig. 1 (Color online) X-ray diffraction patterns for the YBCO/LSMO hybrids with different phase volume ratio and a pure YBCO film of 200 nm in thickness

3 Results and Discussion

Figure 1 shows the XRD $\theta \sim 2\theta$ patterns of the deposited YBCO/LSMO hybrids with different pulse ratio between two phases and a pure YBCO film with 200 nm directly grown on an STO substrate. It is observed that only diffraction peaks that can be assigned to (00*l*)-oriented YBCO, LSMO, and STO, indicating good *c*-axis orientation for both YBCO and LSMO phases. As the YBCO total pulses increases, its (00*l*) peak such as (004) narrows and its intensity increases, indicating the increase of the crystallite size in the growth direction. Due to the overlapping of the (00*l*) peaks from YBCO, LSMO, and STO, it is difficult to find LSMO phases in the present samples. A weak shoulder occurring at the right of the STO (003) peak for the hybrid with high LSMO contents is identified to come from LSMO (003), as the shoulder does not appear in the hybrid with low LSMO contents as well as pure YBCO film. In fact, the existence of LSMO phase and the position of its (00*l*) peak are similar with previous reports of YBCO/LSMO heterostructures on STO substrates [8, 22, 23].

To further characterize the epitaxial quality of the hybrids, YBCO (102) rather than (103) pole figure is measured as there is partially overlapping among YBCO (103), LSMO, and STO (110) peaks although YBCO (103) is the strongest peak aside from (00*l*) diffractions. As can be seen from Fig. 2a–c, the pole figures of all the films are shown with four acutely symmetric peaks located at a titling angle of 45°, revealing that YBCO grows well epitaxially for both in-plane and out-of-plane. In comparison, the pole figure of the hybrid with low YBCO contents shows larger dispersity as compared with the hybrid with high YBCO contents as well as the pure YBCO film. It is observed that the full width at half maximum (FWHM) of the YBCO

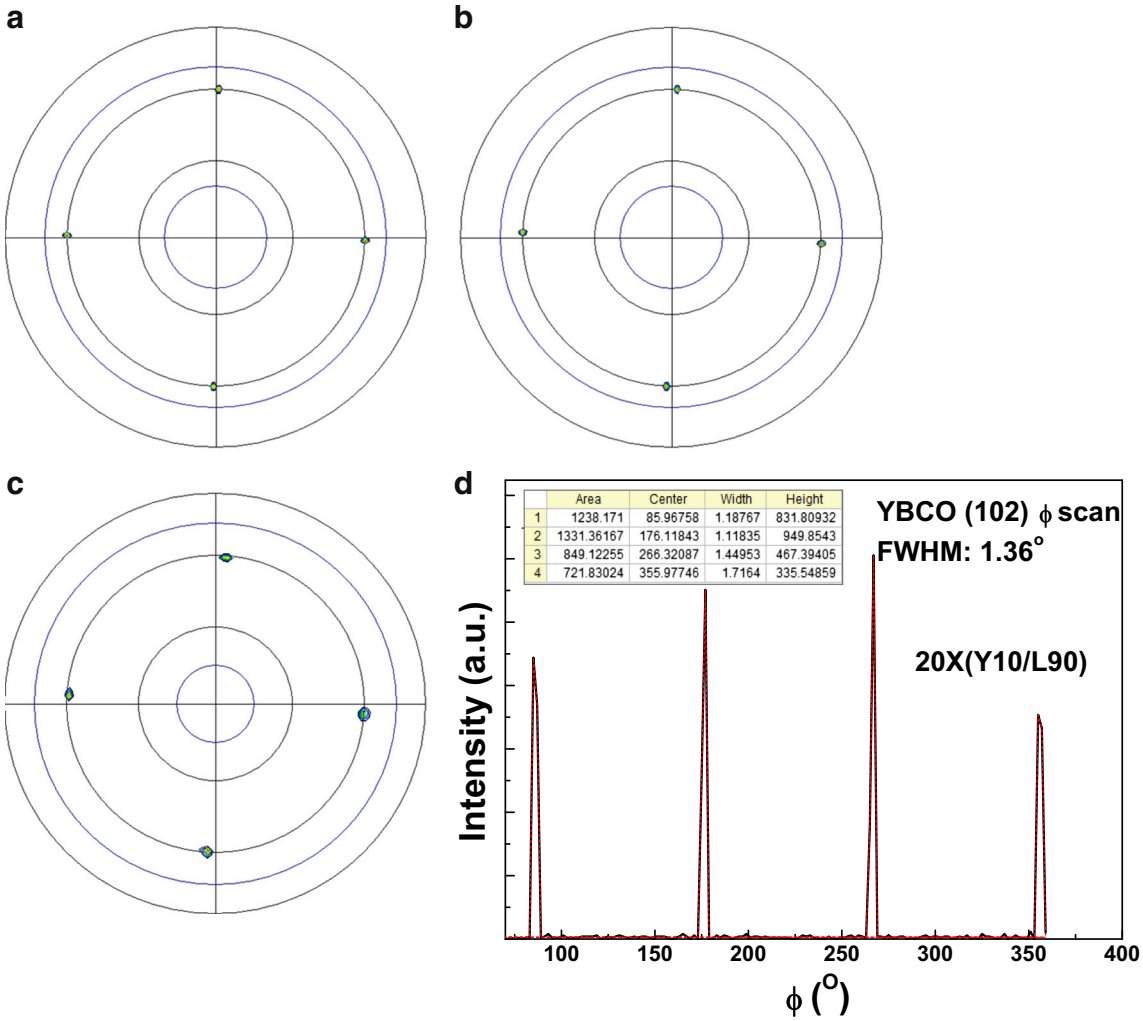

Fig. 2 (Color online) Texture analysis of YBCO lattice in YBCO/LSMO composites. **a–c** YBCO (102) pole figures for the pure YBCO film, the 20 × (Y90/L10), and the 20 × (Y10/L90) hybrid, respectively. **d** YBCO (102) φ scan for the 20 × (Y10/L90) hybrid. Solid red lines are Gaussian fit to these peaks and the fitting parameters are listed in a table as an inset

(102) φ scan for the hybrid is about 1.36° (Fig. 2d), while the FWHMs of the hybrid with high YBCO contents and pure YBCO film are less than 1.2°. The results suggest that the in-plane texture of YBCO lattice in the hybrid gets worse with a reduction of YBCO contents due to an increase of the interface to volume ratio of YBCO phases.

After the establishment of the structural properties, attention is paid to the interplay between superconductivity and magnetism in the hybrids. Figure 3 shows the temperature dependence of reduced resistance of the hybrids with different YBCO contents as well as a pure YBCO of 200 nm and a pure LSMO film of 80 nm. The superconducting transition temperature (T_c) rapidly shifts from 90 to 52 K with pulse ratio of YBCO/LSMO increasing from 9:1 to 1:9, similar to the suppression in T_c that is commonly observed in YBCO/LS(C)MO multilayers and superlattices [24]. The suppression of T_c is mainly due to the presence of a magnetic phase in proximity to a superconducting phase, charge transfer across SC/FM interface, as well as the injection of the spin-polarized carriers [13, 14]. R-T curve of the hybrid with high YBCO contents is similar to that of the YBCO film, i.e., almost a linear dependence on temperature above T_c and below which a superconducting transition begins. However, the transition width of the superconducting temperature ΔT_c for this hybrid, which is determined from the derivative of the $R - T$ curve (the inset of Fig. 3), is as high as 9.1 K. This value is nearly eight times of that of the pure YBCO film, indicating an inhomogeneous suppression of the superconductivity due to the disperse implantation of LSMO nanoparticles. In fact, the most important feature is the insulating nature of the hybrid with low YBCO phases,

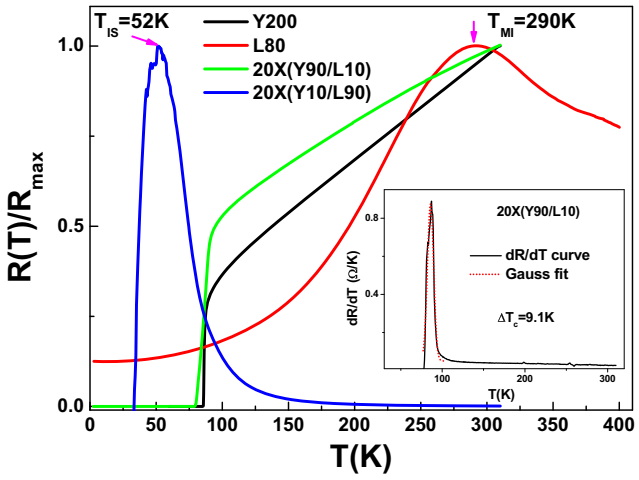

Fig. 3 (Color online) Temperature dependence of reduced resistance of the hybrids with different YBCO content as well as pure YBCO and LSMO films. Inset: derivative of the resistance curve for the 20 × (Y90/L10) hybrid, from which the superconducting transition width is extracted by performing peak fit

which extends the temperature regime from 52 K to room temperature ever higher. This is very different from the R-T behaviors of the pure LSMO film, in which an obvious insulator-to-metal (IM) transition is observed at about 290 K and below this point, the sample is always metallic.

Figure 4a, b give the electric resistance and the magnetic field induced resistance change (right panel), i.e., $\Delta R/R(0)$, where $\Delta R = R(H) - R(0)$, as a function of temperature for the hybrids of 20 × (Y90/L10) and 20 × (Y10/L90). The exerted field is 4 T and its direction is parallel to the c-axis of YBCO and perpendicular to the current flowing direction. For the hybrid dominated by YBCO phases such as 20 × (Y90/L10), the obvious resistance change lies in the region of the mixed vortex state near the onset temperature of the superconducting transition, which is caused by vortex dissipation. It is well-known that for high-temperature superconductors, the broadening of magnetoresistance in magnetic field arises from the thermal dissipation due to the motion of vortices. For the hybrid mainly controlled by LSMO phases, i.e., 20 × (Y10/L90), the temperature dependence of its resistance variation induced by magnetic field presents an oscillating behavior, reflecting the competition between the positive magnetoresistance due to vortex dissipation from YBCO and the negative magnetoresistance due to field-suppressed magnetic scattering in LSMO [8]. The maximum relative resistance change for the 20 × (Y10/L90) sample is less than 1, while this value is as high as 60,000 for the 20 × (Y90/L10) film. This is because the resistance of the 20 × (Y10/L90) hybrid mainly results from LSMO matrix, which is insulating in a wide temperature region from 52 to 310 K.

In order to reveal the origin of the insulating phase in the hybrid mainly controlled by LSMO phases, a three-dimensional variable hopping model (3D VRH) [25, 26] is used to describe the carrier transport in this sample, in which the electrical resistance is given by, $R(T) = R_0 \exp(T_0/T)^{1/4}$, where R_0 and T_0 are characteristic parameters. As one can see from the inset of Fig. 4b, the linear $\ln R \sim T^{-1/4}$ curves covering 70–310 K are observed for the 20 × (Y10/L90) hybrid, indicating that the carrier transport in the present sample is dominated by 3D VRH mechanism. The formation of the insulating state is possibly related to the oxygen vacancies and a resulting decrease of the Mn valence according to Feng et al.'s [27] investigation on ultrathin $La_{0.8}Sr_{0.2}MnO_3$ films by investigating the aberration-corrected scanning transmission electron microscopy and electron energy loss spectroscopy. Due to the existence of the magnetic disorder, the conventional double exchange and phase separation mechanisms are broken and only part of the carriers can be excited and hop between the sites instead of between nearest neighbors. The parameter T_0 correlates with density of state (DOS) at the Fermi level $N(E_F)$ and the localization length

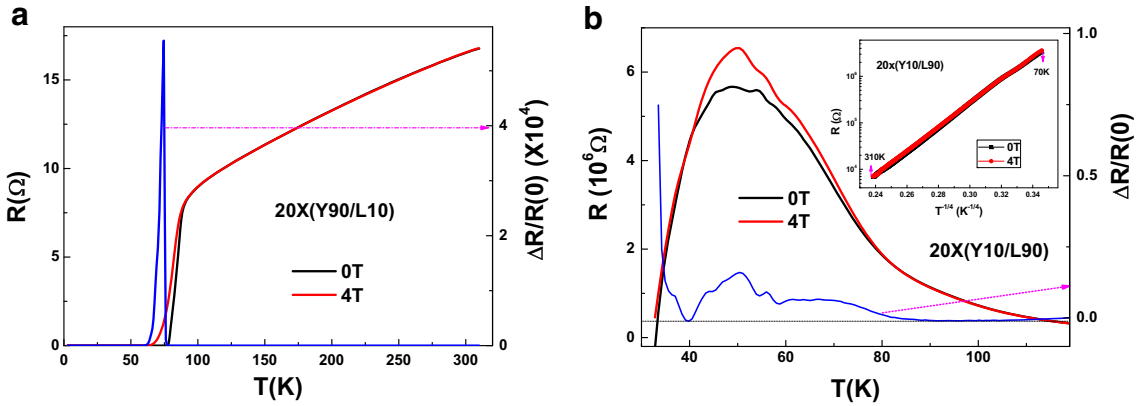

Fig. 4 (Color online) Temperature dependence of the resistance at various magnetic field and the resistance shift induced by the magnetic field (right panel) of the hybrid. **a** 20 × (Y90/L10). **b** 20 × (Y10/L90). **b** The inset is log plot of resistance as a function of $T^{-1/4}$ for the 20 × (Y10/L90) hybrid

ξ_L. According to Mott VRH law, the characteristic length, which is usually used to describe the spreading of the wave function and the degree of the disorders, is expressed by $\xi_L = [21/k_B T_0 N(E_F)]^{1/3}$ [27]. By performing linear fit to $\ln R \sim T^{-1/4}$ curve, we can extract the characteristic temperature T_0. Thus ξ_L can be obtained if $N(E_F) = 2.4 \times 10^{22}$/eV cm^3 of the $La_{0.8}Sr_{0.2}MnO_3$ bulk material is adopted [28]. The estimated localization lengths at 0 and 4 T are 9.32 and 9.42 nm, respectively. Obviously, ξ_L increases slightly with increasing magnetic field, which is a clear indication of field-suppressed magnetic disorders.

To further capture the superconducting and magnetic signals and sense the embedded phases, we perform the magnetic measurements on the present hybrids. Figure 5a, b show the magnetic hysteresis loops of the studied hybrids at different temperatures such as 10 and 100 K. The applied magnetic field is perpendicular to the substrate. The zero field-cooling (ZFC) loop of the 20 × (Y90/L10) hybrid at 10 K presents a typical diamagnetic behavior inherent to epitaxial superconducting films (see the inset of Fig. 5a) [21, 24], while the ZFC loop of the 20 × (Y10/L90) hybrid at the same temperature appears in nearly standard ferromagnetic hysteresis except for the superconducting central peak at zero magnetic field nearby, an indication of the existence of a very weak superconductivity in the 20 × (Y10/L90) hybrid. The superconducting signals are dominant in the hybrid of 20 × (Y90/L10) just as the ferromagnetic signals do in the hybrid of 20 × (Y10/L90) since the magnetization measurement is based on the whole response of the sample. As the temperature exceeds T_c such as at 100 K, the ZFC loops of both hybrids become interesting and abnormal. Firstly, for the 20 × (Y10/L90) hybrid with high LSMO contents, its ZFC M–H loops is ferromagnetic but some important parameters including the ratio of remnant magnetization M_r to saturation magnetization M_s, i.e., M_r/M_s, and the coercivity field H_c decrease as compared with the pure LSMO film (see inset of Fig. 5b as well as Table 1). Its saturation field H_s equals to 5400 Oe, which is nearly two times of that of the pure film, indicating the increased difficulty in magnetization

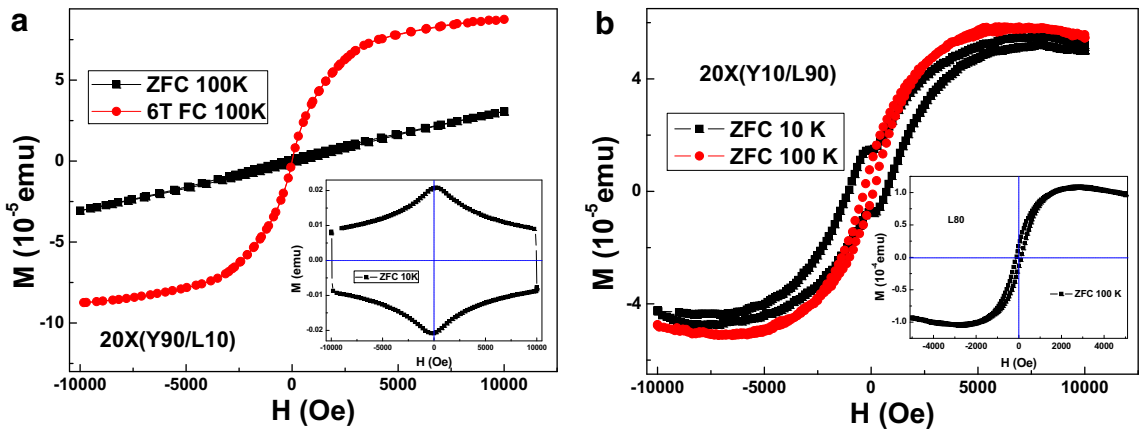

Fig. 5 (Color online) $M(H)$ loops for the hybrid at different temperatures under ZFC and FC modes. **a** 20 × (Y90/L10). **b** 20 × (Y10/L90)

Table 1 Some important magnetic parameters such as the ratio of remnant magnetization M_r to saturation magnetization M_s, i.e., M_r/M_s, the coercivity field H_c, the saturation field H_s for the hybrids with different LSMO contents and the pure LSMO film at 100 K

Sample	LSMO total pulses	M_r/M_s	H_s (Oe)	H_c (Oe)
L80	2000	0.19	2400	195
20 × (Y10/L90)	1800	0.12	5400	110
20 × (Y90/L10)	200	–	>10,000	52

process. Secondly, ZFC $M-H$ loop of the 20 × (Y90/L10) hybrid at 100 K is quite different, which obviously deviates a standard ferromagnetic loop. Its loop exhibits features of superparamagnetic particles characterized by almost zero remnant magnetization and zero coercivity field as well as a very large saturation field [29, 30]. In fact, the present hybrid with low LSMO phase is a diluted system in which ferromagnetic LSMO nanoparticles are dispersed in the YBCO matrix. The spins of these isolated nanoparticles are frozen in a disordered state common to superparamagnetic materials during ZFC process, which is difficult to be magnetized to saturation. To test it, we perform FC $M-H$ measurement by exerting 6T magnetic field in cooling process, which can direct isolated spins in a preferred direction. It is observed from Fig. 5a that the FC $M-H$ loop of the sample is recovering ferromagnetic with saturation field H_s less than 5000 Oe. Similar results were reported in YBCO/Mn(C_O)Fe_2O_4 nanocomposites [17]. As far as we know, the evidence of superparamagnetism in YBCO/L(C)SMO hybrids was not reported before.

4 Conclusions

In conclusion, YBCO/LSMO hybrids with different pulse ratio between two constituent materials are prepared by pulsed laser deposition (PLD), with respect to investigating the novel transport and magnetic properties in two extremely conditions. The individual compounds are structurally phase separated with a high crystalline quality and the epitaxial properties by a combination of XRD $\theta \sim 2\theta$ scans and pole figures. The transport and magnetic studies reveal that the present hybrids with one phase embedded in matrix of another phase produce new and exciting physical phenomena compared to the extensively researched SC/FM multilayers. The magnetic properties of the hybrid with a large YBCO volume fraction are subject to superparamagnetic behaviors inherent to a diluted system although its transport properties are dominated by superconducting YBCO phases. In contrast, the transport of normal state for the hybrid with a large LSMO volume fraction presents an abnormal insulating behavior with 3D VRH conduction dominating this insulating phase while its magnetic properties are dominated by ferromagnetic LSMO phases. Nevertheless, an inhomogeneously suppressed superconductivity and a reduced ferromagnetism are observed to occur in the hybrid with large YBCO and LSMO contents, respectively, as compared with the pure counterparts due to the mutual interactions between two phases. It is believed that these new type of magnetic-superconducting hybrids leaves a trail for novel physical phenomena and advanced applications in the field of superconducting spintronics.

Acknowledgments The authors would like thank Prof. Zhe Li at the Magnetic Materials and Devices of Qujing Normal University for his helpful discussion.

Funding This work is partly sponsored by the National Natural Science Foundation of China (No. 11404005), the Undergraduate Training Programs for Innovation and Entrepreneurship of Anhui University of Science and Technology (No. 201610361282), and the Opening Project of Shanghai Key Laboratory of High Temperature Superconductors.

References

1. Buzdin, A.I.: Rev. Mod. Phys. **77**, 935 (2005)
2. Aladyshkin, A.Y., Silhanek, A.V., Gillijns, W., Moshckalkov, V.V.: Supercond. Sci. Technol. **22**, 053001 (2009)
3. Peña, V., Sefrioui, Z., Arias, D., Leon, C., Santamaria, J., Martinez, J.L., te Velthuis, S.G.E., Hoffmann, A.: Phys. Rev. Lett. **94**, 057002 (2005)
4. Lin, J.G., Cheng, S.L., Chang, C.R., Xing, D.Y.: J. Appl. Lett. **98**, 023920 (2005)
5. Chakhalian, J., Freeland, J.M., Srager, G., Strempfer, J., Khaliulin, G., Cezar, J.C., Charlton, T., Dalgliesh, R., Bernhard, C., Cristiani, G., Habermeier, H.-U., Keimer, B.: Nat. Phys. **2**, 244 (2006)
6. Hoppler, J., Stahn, J., Niedermayer, C., Malik, V.K., Bouyanfif, H., Drew, A.J., Rössle, M., Buzdin, A., Cristiani, G., Habermeier, H.-U., Keimer, B., Bernhard, C.: Nat. Mater. **8**, 315 (2009)
7. Visani, C., Sefrioui, Z., Tornos, J., Leon, C., Briatica, J., Bibes, M., Barthelemy, A., Santamaria, J., Villegas, J.E.: Nat. Phys. **8**, 539 (2012)
8. Chen, C., Li, Y., Cai, C.: Solid State Commun. **152**, 1203 (2012)
9. Uribe-Laverde, M.A., Satapathy, D.K., Marozau, I., Malik, V.K., Das, S., Sen, K., Stahn, J., Rühm, A., Kim, J.-H., Keller, T., Devishvili, A., Toperverg, B.P., Bernhard, C.: Phys. Rev. B **87**, 115105 (2013)
10. Chien, T.Y., Kourkoutis, L.F., Chakhalian, J., Gray, B., Kareev, M., Guisinger, N.P., Muller, D.A., Freeland, J.W.: Nat. Commun. **4**, 2336 (2013)

11. Mani, A., Kumary, T.G., Lin, J.G.: Sci. Rep. **5**, 12780 (2015)
12. Dybko, K., Werner-Malento, K., Aleshkevych, P., Wojcik, M., Sawicki, M., Przyslupski, P.: Phys. Rev. B **80**, 144504 (2009)
13. Penã, V., Visani, C., Barriocanal, J.G., Arias, D., Sefrioui, Z., Leon, C., Santamaria, J., Almasan, C.A.: Phys. Rev. B **73**, 104513 (2006)
14. Habermeier, H.-U.: J. Phys. Conf. Ser. **108**, 012039 (2008)
15. Norton, D.P., Lowndes, D.H.: Phys. Rev. B **48**, 6460 (1993)
16. Suresh, V., Lin, J.-C., Liu, H.-J., Zhang, Z., Chiang, P.-C., Hsun, Y.-C., Chen, Y.-C., Lin, J.-Y., Chu, Y.-H.: Nanoscale **8**, 18454 (2016)
17. Bartolomé, E., Cayado, P., Solano, E., Mocuta, C., Ricart, S., Mundet, B., Coll, M., Gázquez, J., Meledin, A., van Tendeloo, G., Valvidares, S.M., Herreio-Martín, J., Gargiani, P., Pellegrin, E., Magén, C., Puig, T., Obradors, X.: Adv. Electron. Mater. **3**, 1700037 (2017)
18. Wang, J., Tsai, C.-F., Bi, Z., Naugle, D.G., Wang, H.: IEEE Trans. Appl. Supercond. **19**, 3503 (2009)
19. Tsai, C.-F., Chen, L., Chen, A., Khatkhatay, F., Zhang, W., Wang, H.: IEEE Trans. Appl. Supercond. **23**, 8001204 (2013)
20. Wimbush, S.C., Durrell, J.H., Tsai, C.F., Wang, H., Jia, Q.X., Blamire, M.G.: Supercond. Sci. Technol. **23**, 045019 (2010)
21. Chen, C., Chen, H., Cai, C.: J. Supercond. Nov. Magn. **29**, 3127 (2016)
22. Soltan, S., Albrecht, J., Habermeier, H.-U.: Phys. Rev. B **70**, 144517 (2004)
23. Chen, C., Li, Y., Wang, B.: Solid State Commun. **161**, 1 (2013)
24. Przyslupski, P., Tsarou, A., Dluzewski, P., Paszkowicz, W., Minikayev, R., Dybko, K., Sawicki, M., Dabrowski, B., Kimaball, C.: Supercond. Sci. Technol. **19**, S38 (2006)
25. Ovsyannikov, G.A., Denisuk, S.A., Bdikin, I.K., Ivanov, Z., Claeson, T.: Physica C **616**, 408 (2004)
26. Ovsyannikov, G.A., Constantinian, K.Y., Kislinski, Y.V., Shadrin, A.V., Zaitsev, A.V., Petrzhik, A.M., Demidov, V.V., Borisenko, I.V., Kalabukhov, A.V., Winkler, D.: Supercond. Sci. Technol. **24**, 055012 (2011)
27. Feng, Y., Jin, K., Gu, L., He, X., Ge, C., Zhang, Q., He, M., Guo, Q., Wan, Q., He, M., Lu, H., Yang, G.: Sci. Rep. **6**, 22382 (2016)
28. Woodfield, B.F., Wilson, M.L., Byers, J.M.: Phys. Rev. Lett. **78**, 3201 (1997)
29. Xu, J., Howson, M.A., Hickey, B.J., Greig, D., Kolb, E., Veillet, P., Wiser, N.: Phys. Rev. B **55**, 416 (1997)
30. Eerenstein, W., Hibma, T., Celotto, S.: Phys. Rev. B **70**, 184404 (2004)